Macro-Scale Findings of the DebriSat Debris Field Obtained from X-Rays of the Catch Panels

Anthony Allen [1] and John B. Bacon [2]

[1] University of Florida, 1949 Stadium Rd, Gainesville, FL 32611 USA, allen.anthony96@gmail.com
[2] NASA Johnson Space Center XI-5, 2101 NASA Pkwy. Houston TX 77058 USA, john.bacon-1@nasa.gov

ABSTRACT

The DebriSat project analyzes the debris from a hypervelocity impact test conducted on a 56 kg-simulated satellite target in 2014. Its purpose is to generate a comprehensive database of the size, mass, material, shape, and the radar and optical properties of fragments generated from orbital collisions of modern-built spacecraft. Three hundred ninety-one foam catch panels from the DebriSat test have been X-rayed to locate the particles within them for subsequent extraction and assessment. The data from the tens of thousands of extracted particles has heretofore been the focus of the debris assessment. The work presented here connects the X-ray sample location images to reconstruct the 3D distribution of the entire fragment cloud. Although some errors are inherent to the process, this 3D database is valuable for qualitative studies of size and energy distributions. Further, the 3D database can indicate the extent of bending or breaking of the fragments as they decelerated to full capture. By virtue of its full sphere perspective, the 3D database allows graphical insight to the physics of the collision and breakup. This 3D representation has been developed as a "point and click" graphical interface to retrieve the full data set on individual recovered and assessed fragments within the growing database. Overall, this macro-level screening technique has added enormous insight to the experiment in unexpected ways.

1 BACKGROUND

Following the 2007 collision of the Iridium 33 and Cosmos 2251 spacecraft, the debris distributions of the two spacecraft exhibited qualitatively different behaviors. Although, Cosmos 2251 followed the predictive models of debris size and speed distribution, Iridium 33's debris field did not. In an effort to determine the statistical model for the breakup of such modern spacecraft, in April 2014 the NASA Orbital Debris Program Office (ODPO), the Air Force, the Jacobs Engineering Group, and the Aerospace Corporation pooled resources with the University of Florida (UF) to conduct a hypervelocity breakup test in a foam-lined chamber at the Air Force Test Center's Arnold Engineering Development Complex hypervelocity impact facility near Tullahoma, Tennessee [1].

The data collection process employs an X-ray machine to scan foam panels extracted from the chamber post impact. This X-ray step is unique in the history of hypervelocity tests and is intended solely to accelerate the process of finding and extracting the captured fragments. Prior to this reported activity, these processed images were used only to aid student technicians in their attempts to extract embedded debris [2]. The current study seeks to use these X-ray images as an independent comprehensive record of the size and spatial distribution of all captured particles. The shape and location data are not as complete as the material, mass, color, and full dimensional data for the extracted debris. Further, this alternate method of photo analysis has certain statistical biases that must be accounted for. However, the X-ray images provide fast and comprehensive insight into many aspects of the debris cloud that cannot be attained in the particle-centered database records.

2 APPROACH

Students at the University of Florida built a collection of 391 foam panel X-ray images over a span of 4 years [3]. Of these, 275 had debris items embedded in them prior to extraction. All work conducted in the creation of this paper is a product of the additional analysis of this image set. The current expanded methodology – invoking photo analysis of such X-ray images – has led to an improved analysis program, soon to be implemented, which takes greater advantage of a replacement X-ray machine. The replacement unit is a surplus airport luggage scanner that allows the analysts to build multiple views through the foam. It provides the possibilities of adjustment to distinguish metallic-from non-metallic-debris, to resolve the cavities left by the debris as it decelerated (thus mapping the energy dissipation history), and to do preliminary multidimensional shape assessments of every debris item from numerous vantage points, similar in principle to a Computer-Assisted Tomography (CAT) scan. At time of publication, the

installation of the new X-ray unit is still in work. The bulk of this paper addresses the techniques developed for the original set of X-rays using the former equipment.

2.1 Fragment Detection Algorithm

MATLAB offers an array of functions to identify object edges in an image. The accuracy of each method was determined by analyzing the visual completeness of the fragment cluster as well as a comparison to fragments directly extracted from the UF database. A method called Canny Edge Detection[1] (Canny) was implemented to identify the outer edges of the debris items within stitched[2] full-panel images. The Canny algorithm was preferred for this application because it represented the best-fit edge of an object with a single pixel thickness [4]. This enabled researchers to collect data on fragments without significantly distorting their size or shape. Many other detection methods located edges as a thick border surrounding the identified object.

The Canny algorithm first implements a Gaussian filter technique that smooths grayscale images for easier processing. Next, the image gradient is analyzed to determine the best-fit edge for all embedded fragments. Canny uses a double threshold to eliminate any pixels that fall below (darker than) a grayscale value of 0.036 or higher (brighter than) than 0.078, with gradient tests on adjacent pixels determining the retention of those in between. This compares to the original single-threshold process that unnecessarily filtered out a larger volume of data, looking for the bulk shadow of the object rather than its true edge. The lower threshold value is determined by calculating 25% of the mean pixel variation in each image. The larger value is determined visually. With fragments detected, the hollow boundaries are filled in to provide an accurate solidity of the fragments [3]. The output of the Canny algorithm is a binary image where pixel values equal to one comprise the overall area of detected debris items. Figure 1 depicts a typical gray-scale stitched full panel and the binary output produced by the Canny function.

Using the ***regionprops*** MATLAB function, geometric and spatial location data are collected from the identified fragments. Most noise is filtered out by eliminating detected objects smaller than 10 pixels in their longest dimension. The X-ray system's image plane engenders a conversion factor of approximately 9.5 pixels per millimeter. This factor is recalculated for every image, accounting for minor set-up variations in the X-ray camera.

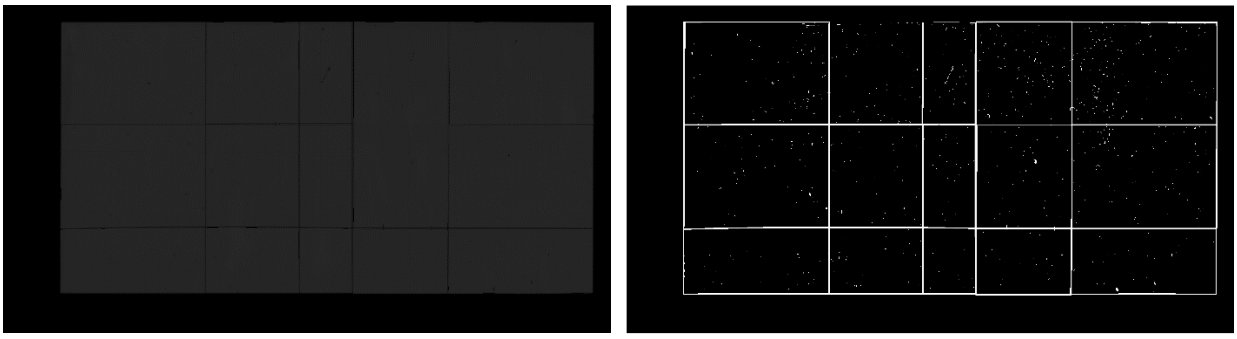

Fig. 1. The figure to the left depicts the original gray-scale "Stitched Full-Panel" of panel DSF285. The binary figure on the right is the Canny output for panel DSF285. Post processing images of this panel can be seen in Fig. 2.

When panels are X-rayed, a grid is used to hold them stationary. This grid is evident in the X-rays, as seen in Fig.1, and identified by the algorithm as a very large fragment. The grids in the X-ray images are removed by eliminating "fragments" with an area greater than 60,000 pixels^2, roughly 6,300 mm^2. This, of course, is much greater than even the largest fragments. The remaining binary shadowgraphs include fragments ranging upwards from 1 mm. Although each millimeter constitutes over nine pixels, and can thus reveal even smaller particles, the data is

[1] The Canny edge detector was developed by John F. Canny in 1986. It uses the calculus of variations to optimize edge detection in complex image fields and is used widely in computer vision systems [4].

[2] Since the image plane is much smaller than a single panel, 12 images are taken of each intact foam sheet [2, 3]. The images are then "stitched" together to build a composite "full-panel" view. A software algorithm is used to determine the locations of debris fragments within each panel and highlight them for students to identify the particles for extraction. The algorithm prior to the current research provided little to no debris size or shape statistics from such imagery.

somewhat noisy, and for the purposes of this research, the data set is truncated at 1 mm. It is a simple matter to explore smaller items in the X-ray, however. Geometric properties along with orientation and location within a panel are collected for each fragment. Using geometric and spatial location data, fragments found in the shadowgraphs can be correlated to the same fragments in the UF database with limited human input.

2.2 3D Rectilinear Scatter Plot

Under the current research, the software records size, orientation, and shape data for every particle and the X-ray debris locations are organized into a 3D rectilinear plot. For development purposes, the fastest visualization technique plots spheres of the same cross-sectional area as the debris item, rather than rendering the full 2D shadowgraph oriented in 3-space, although the latter process is easily accomplished at some expense of display time. Plotting routines can easily correlate color with specific layers, sizes, or even orientations of the debris. The MATLAB ***regionprops*** algorithm determines the centroid location of each debris item relative to the embedding panel. The top left corner of each panel identifies the local point of origin. Our process to map the debris to global coordinates revealed an uncertainty in the X-ray imaging step that occasionally ambiguously oriented 60×120×2.5 cm panels within the four possible orientations of that specific geometry[3] [5]. When viewing the X-rays as a landscape image, the long horizontal side is defined as the local panel x-axis. The positive y-axis begins at the top left corner and continues in increments down the height of the image following the MATLAB image indexing system. The point of origin, x-, and y-axes are depicted in Fig 2.

The test chamber established the global Cartesian reference frame. A unique transformation of the local panel coordinate system to the global system is required for every panel. The center of the pre-impacted DebriSat spacecraft is the point of origin of the global frame. Downrange (the direction of the impacting projectile's flight) is the +Z-axis. Upwards is the +Y-axis. Towards the right, when viewing the chamber from uprange to downrange, is the +X-axis. All coordinate systems from the foam panels are then transformed to this Cartesian reference frame. All imaged fragments are thus located uniquely in the global reference frame. A 3D scatter plot is generated with the collected data (Fig. 3).

2.3 Spherical Scatter Plot

To better inspect for asymmetries and inhomogeneity in the breakup, a 3D spherical model is created. The solid angle of each debris item is acquired using standard Cartesian-to-spherical coordinate conversion equations. The polar coordinates of each fragment are plotted to lie on spherical surfaces of uniformly spaced shells 10 mm apart, beginning with the front panel's surface at an arbitrary 1000 mm. The shell to which the fragment is mapped correlates with the layer of foam in which it is found. Deeper panels map to larger spherical surfaces. This gives the satellite pieces a debris cloud map more representative of the expanding debris cloud prior to capture, which can be seen in Fig. 5 and Fig. 6. Such representation creates insight to spatial density and anisotropy of the breakup.

2.4 Software Methods to Cross-Link a Particle's Database Record to its Image in the X-ray

Two algorithms were prototyped to crosslink debris items found in X-rayed panels with extracted fragments. One variant, the Forward-Matching Method, started with a single database fragment entry and worked to identify the same fragment in its X-ray image. The second variant, the Backward-Matching Method, started with a MATLAB ***brush*** function's screen selection from the X-ray image (and especially, from the full Cartesian map of the foam X-rays) to find associated data in the full database for the small selected region.

The Forward-Matching algorithm was the more heavily developed during this project. The primary reason for this software is to allow the team to assess whether there is any bias in the orientation of the fragments with respect to their trajectory through the foam. This method questions if two-dimensional or one-dimensional objects, such as

[3] Inspection of the X-ray process revealed an ambiguity in the work instruction that translated to an infrequent ambiguity in panel orientation that did not anticipate the global reconstruction of the images into a full mosaic. The result is, even though properly placed into the chamber reconstruction, some of the puzzle pieces occasionally end up upside down or rotated 180 degrees. Nonetheless, research to support this current paper proceeded since the goal was to establish a general large-scale understanding of DebriSat's breakup. Techniques to identify and rectify such orientation ambiguity are in work, and the database can be easily updated once each panel's orientation is confirmed. The expected capability of the new X-ray scanner to map the penetration cavities should aid significantly in orienting the panel with respect to the explosion. Such information is currently gleaned from visible light photographs of the panels.

flakes and wires, align in fully random orientations or in minimum-drag orientations as they decelerate. This drag-induced orientation bias affects the statistics of particle size if the X-ray images only capture systematically oriented fragments. Additionally, this tool is intended to assist easily in determining the bending of any distorted objects relative to the flight path, to determine if the bend is caused by the fragmentation event or by the capture event.

The Forward-Matching Method is accomplished by first picking an object from the UF database with size, mass, optical properties, and embedding panel identified. The algorithm then finds the panel's processed X-ray image. This can be done with reasonable geometric precision for the majority of the panels that are unambiguously oriented. This is because a 30× reduction in location uncertainty is recorded for each extracted fragment in the UF database, by virtue of the particle's association with coordinates of a 5×6-cell grid placed over the panel during the X-ray to assist in stitching the many smaller photos together. This same grid pattern is subsequently used to identify the approximate location of the debris item within the panel as the fragment is entered into the database. Using a fragment's coarse grid location, the crosslinking algorithm identifies X-ray images of approximately the same size particles within that grid location. Because of the previously discussed ambiguity of the panel orientation, the algorithm currently searches for the desired fragment in all grid locations associated with the four possible panel orientations, in case no close match is identified in the assumed orientation. Images of the limited number of potentially similar X-ray items are displayed for comparison to high quality fragment images from the UF database, and the user then manually assigns the match. Generally, this misorientation is rare, however.

The second version of the software is envisioned as a powerful data exploration tool, once the full database is complete. The relative sparsity of the data for extracted particles with respect to the bulk X-ray data makes this technique difficult at present. This method's intent is to look down a trajectory of a large fragment and explore the fragments close to it along the flight path – even across several layers of foam – to explore whether the material properties would indicate that the smaller objects might have been shed during the capture process. It may be able to assist in reconstructing the dynamics of how specific components fragmented and seek trajectories that are not purely radial from the center of the inertial rest frame of the spacecraft. (This latter effect is to be expected from conservation of momentum but is difficult to map *a priori*.)

3 RESULTS

3.1 Enhanced Edge-Finding Algorithm and Relative Success to the Old Method

In correlating the X-ray data set to the full database of samples extracted from such panels, it quickly became evident that the prior X-ray particle identification methods were not capturing everything that the students eventually extracted from the panel. Thus, the revised Canny system was developed to identify more completely what was contained within each panel. In addition to building a better 3D map and size distribution of the data for the current study, this enhancement has the obvious additional benefit of more accurately identifying the particles for extraction. This algorithm is expected to streamline the extraction process with more complete identification and fewer false positives, leading to direct and complete extraction.

The Canny algorithm improved the overall count of detectable debris items to 103% (Eqs. 1 and 2) of those identified in the UF database within the same size range. Further, while the UF database accounts for fragments as small as 2 mm, the imaging method can identify those 1 mm or greater. A visual comparison of these two methods is in Fig. 2 and Fig. 3. Some fragments are still undiscovered by this algorithm. Many of the panels have a film of darkening on them as well. This darkening material is thought to be vaporized satellite components [6]. Because of this, some fragments are hidden under a layer of dark vapor creating an indiscernible or indistinct edge. In addition, the darkening is easily mistaken as a solid debris item because of its varied thickness throughout some panels. To negate these inaccurate discoveries, each image is manually analyzed, and areas with significant darkening are zeroed out. (Patterns of systematic noise can be zeroed out by removing fragments less than 1 mm.) The replacement of the stitched X-ray system with the more flexible luggage scanning technology is expected to allow significantly better filtering algorithms and automation.

$$Total\ Fragments\ = database\ fragments - fragments\ in\ a\ cluster + total\ number\ of\ clusters \tag{1}$$

$$\%\ detected = \frac{Total\ Fragments}{Xray\ Fragments} * 100 \tag{2}$$

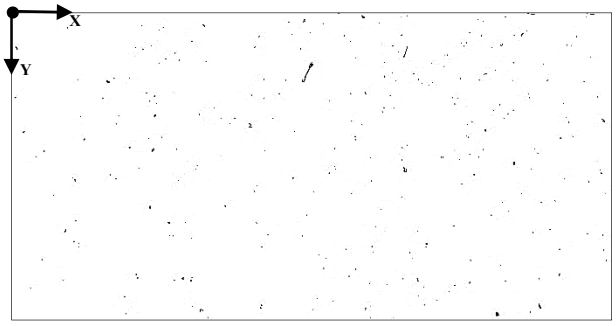

Fig. 3 depicts panel DSF285 after processing from the original X-ray code.

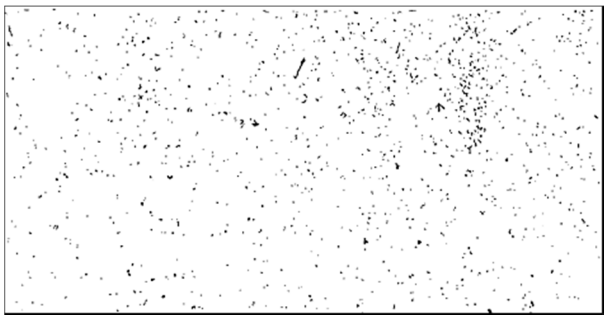

Fig. 2 depicts panel DSF285 using the Canny Edge Detection method.

3.2 Rectilinear Scatter Plot

The Cartesian scatter plot is created to visually inspect debris item locations within the test chamber. The model makes it possible to pinpoint where every fragment landed in the chamber (Fig. 4). The progress of the project and completeness of (or conversely, voids in) the data set can easily be tracked with this visual aid. The left-most part of the chamber, as seen in Fig 4, is mostly empty. Other areas appear lightly populated or have taken the brunt of the debris material. This scatter of debris density is a product of many factors. The extraction team at UF localized much of their search to areas downrange of the impact as that area was expected to be more densely populated. These areas have been the primary focus for the first part of the extraction process due to the complete set and dense population of panels in that row. Panels directly surrounding DebriSat ─ the mostly empty section in Fig. 4 ─ were shattered by the impacting fragments and gas cloud. These panels need to be pieced back together before researchers can add them to the scatter plot. Separate "puzzle piece matching" efforts will be needed to complete this step. Without such reconstruction for the chunks, the debris distribution is blurred, as a "grey background," rather than a precisely located fragment cloud. Much of this work can be done retroactively, again using the X-rays themselves, which reveal the shape and size of the individual chunks.

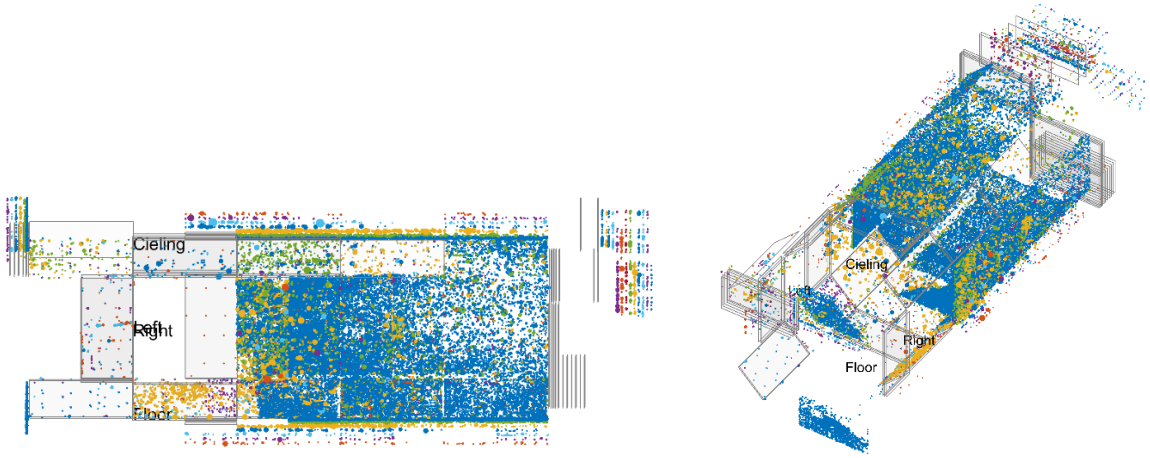

Fig. 4. 3D rectilinear plot using a parent Cartesian coordinate system. This representation allows a good perspective of the chamber itself but is not necessarily the best representation of the debris field in 3-space. Colors in this representation are assigned by layer but can easily be reassigned to vary with fragment area, characteristic length, spatial density, eccentricity of best-fit ellipse, total energy, or any other value that can be derived from fragment shape, size, and location.

3.3 Anisotropy Plot

The 3D spherical distribution model makes it possible to analyze the directionality and anisotropy of the plume. The current incomplete dataset indicates the debris items landed densely along the velocity vector of the projectile.

However, the lack of intact panels laterally surrounding the pre-impact location of the satellite indicates a more catastrophic release of energy. Many panels were destroyed or are missing in this area as well as at the end of the test chamber. Although the conservation of momentum dictates that most debris lies downrange, a significant and interesting fraction of debris items lie uprange of the impact.

Fig. 5. 3D disbursement of fragments at a uniform radial distance from the spacecraft.

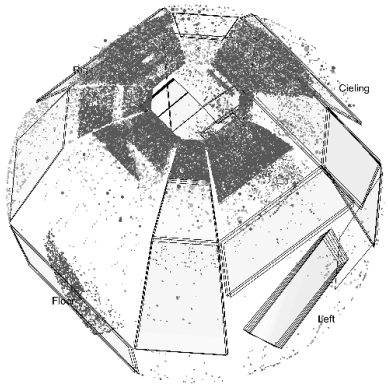

Fig. 6. 3D disbursement with missing panels identified (Linear borders: a better plotting algorithm will map these to a spherical surface).

3.4 New Power Law(s) and Velocity Distributions

Within just the currently imaged subset of panels, 62,000 images of debris at all sizes can be analyzed. Using the major axis lengths of each fragment collected from the edge detection algorithm, the size distribution can be analyzed in power-law curves. Such size distributions are a major goal of the DebriSat experiment, and the X-ray technique provides immediate insight into the final answer to this question, even accounting for uncertainties in bulk statistics resulting from potential biased longitudinal alignment of the particles into the foam as they decelerated. When analyzing the entire range of collected fragments, the power law equation closely models existing data for very small particles. However, the more damaging fragments larger than 100 pixels (11 mm) follow a different law.

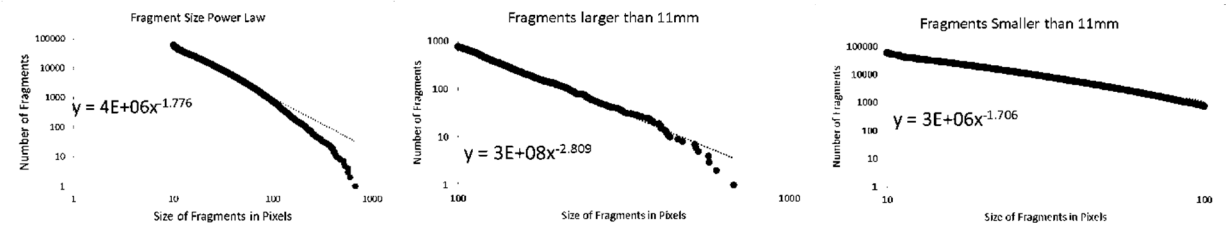

Fig. 7. Overall plot shows a "knee" in several cuts at the data. The "Fragment Size Power Law" plot on the left depicts the number of fragments vs their maximum dimension for the entire range of debris items. The "Fragments larger than 11 mm" plot is the same analysis but localized to particles on the right side of the "knee." The third and final plot depicts the remaining fragments smaller than 11 mm.

Note: there may be a bias towards embedded small fragments and a sparsity of comparable data for larger particles in this method, since the larger ones may be the cause of panel fragmentation, especially downrange where few panels survived. Additionally, some of the biggest particles may have gained little enough velocity and met enough gas resistance to ultimately end on the floor of the chamber, not embedded in the foam. This was noted for the especially large objects that would bring up the far-right side of the curves in Fig. 7. In the future, such bias can be discerned in the surviving panels by exploring whether the relative ratio of large particles to small particles increases as the plume approaches the destroyed panels. Figure 7 depicts the power laws generated by the entire range of fragments as well as fragments greater and less than 11 mm. A dramatic change in physics may be present for fragments on either side of this dividing region, and evolving focus of the debris extraction and characterization and of the image analysis will emphasize particles in this size range to better understand the phenomenon.

3.5 Aspect Ratio

The overall purpose of this research is to record and to analyze both size and shape statistics of fragments. The provided figures account for the simplest measure of non-spherical shape: the elliptical eccentricity of the best-fit ellipse with common area and moments of inertia to the imaged silhouettes of the debris. Figure 8 depicts the minor-to major-axis ratio across distinct size ranges, revealing some macro-scale shape physics. It also shows that fragments smaller than 30 pixels are primarily spherical. Between 30 pixels and 100 pixels, the fragments favor a more elliptical shape. Whereas, debris items larger than 100 pixels have a wide variance in shape. When plotting the shape variance in the UF database and comparing it to the X-ray data, the two plots do not match. Further analysis will need to be conducted to ensure the equations used are equivalent.

Although not yet characterized, we expect a skew bias in the X-ray dataset that can potentially misrepresent the actual shape of the fragment. The particles are believed to orient with minimum cross-sectional area into the flight path, this presenting a bias in the images to show only the maximum area when viewed through the panel. Early evidence supports but does not yet confirm this assumption. The path forward uses the measured data for each extracted fragment. Using the cross-link software methods discussed above, we can do a head-to-head comparison between actual fragments and X-ray-represented data for a more accurate analysis. Further, the new X-ray facility (the re-purposed airport luggage scanner previously mentioned) will be able to get a rudimentary 3D shape carving of each particle with multiple perspectives that can immediately characterize any orientation bias.

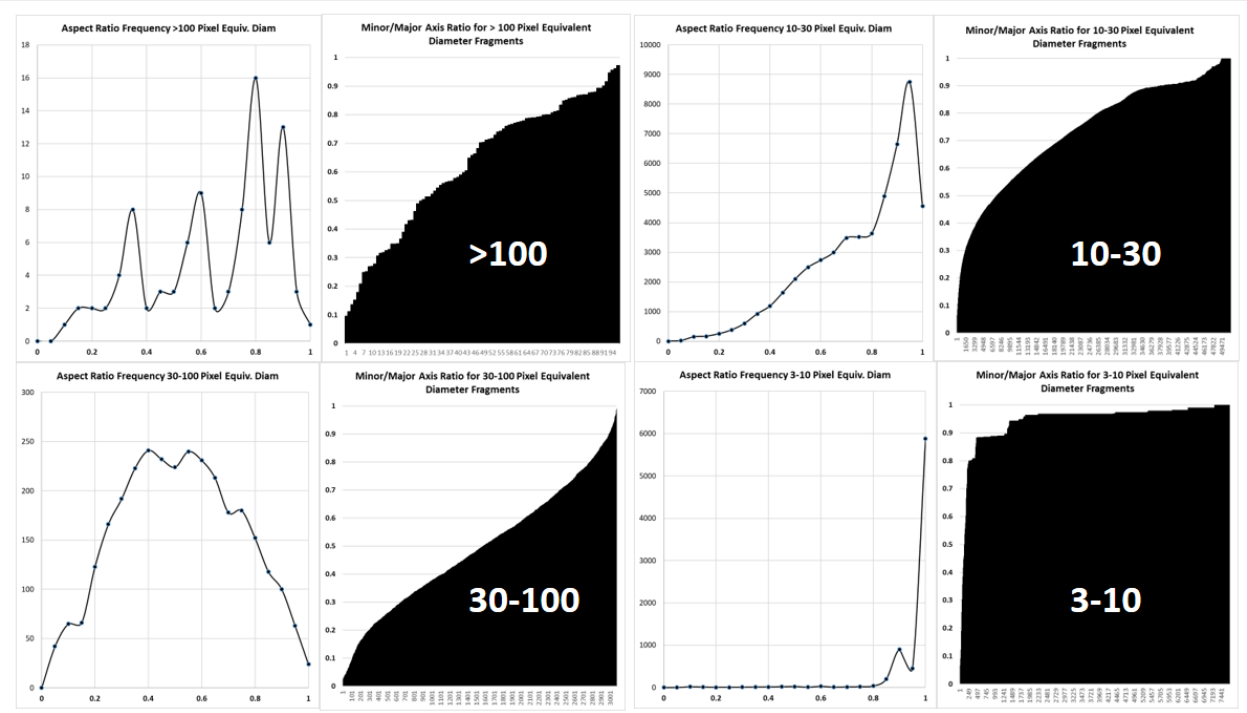

Fig. 8. The statistics of the fragments' minor axis-to-major axis ratio is plotted, grouped in half-decades of individual fragment area in pixels. Area groupings are labeled in white in the black bar chart area. This ellipsoid data (including the ellipse's orientation) is a by-product of the existing method to locate the particles. An equivalent ellipse for each irregular object is an automatic product of the MATLAB ***regionprops*** image assessment function used to identify the fragment locations.

4 DISCUSSION

This methodology augments but does not replace the "ground truth" of the extracted fragments, for which so many more data fields exist. The graphical analysis within the X-ray image however, does add significant insight into and context for the more precisely measured individual fragment properties and can greatly automate and expedite the

broader understanding of shape, size, and trajectory distributions. The detailed assessments below address the specific strengths and weaknesses of the X-ray image analysis method for debris statistics, and recommended process improvements for future experiments.

4.1 Edge and Trajectory Detection

The improved Canny algorithm provided significantly greater visibility of the X-rayed fragments. However, some inaccuracies are still present. The X-ray image plane appeared to have small specs on it. These specs appeared as repeating patterns throughout a given panel. Since each stitched image is comprised of 12 separate X-rays, the pattern was visible on each of these within a full panel. The systematic error was initially theorized to be dust or a variant of it. However, further investigation showed an inconsistent pattern from panel to panel. It is possible the image plane was cleaned at various instances, thus allowing new patterns to form. Another possibility is the partial loss of a pixel's properties due to the compression of the image [7]. Further, the rectangular-format image plane and point source of the prior X-ray system led to a 3D distortion of the actual location of the particle in the thick panel above the image plane. Sometimes, up to four separate projections of the same particle were visible close to the corners of the image plate, as the same particle projected into different quadrants. The line-scan format of the anticipated luggage scanner technology avoids such issues and creates a uniform image built one-pixel row at a time, more like a photocopier scan than a photograph, a parallel projection vs. the prior perspective view.

When locating fragments relative to the test chamber, the local coordinate system of every panel is the same. However, the individual transformation to the global chamber coordinate system is unique to each panel. Because many panels were violently displaced during the impact test and a small flaw in the standard imaging instructions allowed it, an ambiguity in panel orientation occasionally resulted. The data analysed in the scope of this paper is largely unaffected by this ambiguity. However, future work will require a more precise dataset. Current efforts are under way to resolve this ambiguity. In one method, the trajectory cavities generated by debris items are under study in an effort to derive kinetic energy correlations for the particles. Equation (3) can be used to determine the angle a fragment entered the foam. This angle can be represented in MATLAB with a line along the fragments flight path. Lining up the fragments' flight path with their point of origin (DebriSat) ensures that the panels are aligned correctly.

$$Angle\ of\ Impact = \sin^{-1}\frac{radial\ distance}{downrange\ distance} \tag{3}$$

Using the prior X-ray facility, depth of the fragments within their embedding panel could not easily be measured. Debris depth is currently estimated at the center of any given foam panel. The new X-ray facility, when operational, will explore the capability to resolve true depth in the panel. Catch panels can be imaged at different angles and compared to reveal an object's depth and essential shape with as few as three scans. This approach is a rudimentary form of CAT scan. With an unlimited budget, a full CAT scan could prove very useful for this research as well, but preliminary studies reveal that the bulk of the desired insight can be achieved with far simpler technology. This new 3D-shape-and-location method is the subject of immediate future work.

4.2 Geometric Reconstruction

The test chamber layout and placement of DebriSat prior to the breakup largely reflected the initial assumptions of how fragments would disperse. The length of the chamber indicated the assumption that fragments would primarily generate downrange of the spacecraft. While this assumption did prove correct, the width of the chamber may have been undersized for the total energy released into the foam catchment. While the dataset for these plots is incomplete, post impact analysis of the test chamber indicates that many panels in the lateral rows are either missing or severely damaged. If 3D reconstruction of the debris field is important, then the individual panels should have more, unambiguous clues as to their original orientation in the tunnel. Some techniques are emerging from the DebriSat experience.

The extraction team at UF has a large collection of broken panels containing massive amounts of debris items [2, 3]. Many of these foam chunks are less than 10 cm in their longest dimension. Creating an algorithm to fit most broken pieces back together and identify their original location prior to impact will provide data to determine the average flux in this lateral region. Prior to extraction, multiple images are acquired from each broken panel. Since these images are taken with a ruler next to the foam piece, they can be scaled for accurate representation during reassembly (Sadly, the current imaging technique requires manual scaling of each image. The X-rays themselves are

better scaled than the documentary photographs.) The combination of shape and size creates a reconstruction problem akin to solving a 3D jigsaw puzzle. Fortunately, the eight radial sectors of the tunnel were made of foam using only four colors, reducing the ambiguity by a factor of four. The panels had different thicknesses and densities at each layer, allowing some insight into the layer at which the original panel lay. Further, the serendipitous deposit of darkened material from the plume helps to identify the front panel from the identically classified panel behind it (color, density, and thickness are the same for the first few layers.) Finally, the direction of the trajectory cavities inside the foam, and the surplus of entry-hole count on the front side to exit-hole count on the backside can help to orient the parent panel of the fragment. All of this can refine the panel chunk's location and orientation in the global coordinate system, such that spatial densities and impact energies can be accurately determined. All of these techniques, currently under development, can serve to solve the 3D jigsaw puzzle. While no X-ray data exists for foam chunks smaller than 25 cm, this jigsaw reconstruction technique can still approximately locate the chunk as a whole. Because no further spatial resolution is possible, the recovered debris from such chunks is added to the general "white noise" statistics of the fluxes in that sector or layer.

4.3 Data Analysis

When analyzing the power law curve over all fragments, the size distribution closely models the preexisting data, Fig 7. However, a drastic change is present for fragment larger than 11 mm. The crosslinking algorithm is being used to compare X-ray fragments to database fragments. Upon completion of this step, power laws can be compared from both datasets to validate the accuracy. The new scanner may help significantly to reconcile debris orientation biases.

The power law describing the size distribution over all the analyzed fragments closely resembles prior data for several reasons. Only 1.24% of the debris items under consideration are larger than 11 mm. Consequently, the overall curve biases in favor of the smaller fragments (those with a major axis less than 11 mm). While finding a power law similar to previous models supports a relative accuracy of the analysis, the presence of a variance between the size groups implies some correlation with Iridium 33's debris cloud. While the trend of the data appears accurate, there is some potential for error. The most concerning of these error sources is the orientation bias of the fragments. While the future X-ray facility will allow enough 3D shape reconstruction of the fragments within the foam to determine unbiased shape statistics, efforts are ongoing to determine the extent of this bias by cross-referencing a large sample of the database items' 3D shapes to their X-ray silhouettes.

Although there will always be some ambiguity in any individual particle's shape, it is the statistical distribution of cross-sections and shapes that is the true goal of such research. Thus, to the extent that the biases and inherent error bars are understood, in such randomized debris distributions, the use of X-ray silhouettes of the entire debris field is a powerful and rapid way to gain insight into the size and shape statistics of debris that may impact a spacecraft.

The NASA ODPO specialists plan to model fragments with a limited set of representative shapes, as an averaged/simplified model of the true shape based on all dimensions. Such shapes have typically two to three parameters that uniquely fit them to the real image, such as area and eccentricity. Angular orientation information is also useful but expected to be randomized). ODPO considers it necessary to model only three different shapes: a sphere, a rod, and a plate. These shapes appear to be the most relevant statistically. [9]. Prior ESA work [8] has studied ellipsoids of revolution as a generic representation of non-spherical debris. Optimally, both concepts can be fit to the silhouette data to understand the residual errors in such models, as "fractal" indents and bulges of the true shape around the simplified parametric model. Each model can then generate statistical plots of the shape parameters, such as those shown in Fig 8. Fortuitously, the ***regionprops*** function of MATLAB already optimizes the ellipsoidal fit to any silhouette, so no coding is needed for the ESA model.

Of course, this generalized shape set will carry some (often-significant) error in true impact damage potential simply because the modeled shape will have different sharpness and true cross-section than the actual ragged fragment. Thus, due to the inherent errors of the simplified models, there can be a comparable amount of error in the actual statistics of the real shape-measured dimensions.

5 CONCLUSION

The X-ray of catchment panels is a useful "big picture" contextual view of any hypervelocity experiment, showing numerous geometric effects not visible immediately in the database of individual debris items, while rapidly gathering shape, size, and orientation bulk data. In particular, the errors associated with this rapid bulk method of data gathering evidently are well within the intrinsic net error of the models that are to derive from it. Together these

two data-gathering methods can be used to build a more complete understanding of hypervelocity breakups. The technique lends itself to near-instant size and energy distributions, spatial anisotropies, and detailed physics of capture, as a fortuitous by-product of the process of more rapidly extracting the fragments for study. Near-term enhancements using a surplus luggage-scanning unit are expected to add knowledge of material type, three-dimensional shape and volume, complete spatial location, and history of capture events such as bending and fragmentation within the catch panel. All this can be learned prior to fragment extraction. With improvements and recommendations that have evolved from this initial study, we expect that debris cataloging from hypervelocity impact tests of spacecraft can be greatly enhanced and accelerated relative to current techniques, and extended to size ranges below those that can be practically measured via extraction.

6 REFERENCES

1. Polk, E.M. and Roebuck, B.E. "DebriSat Hypervelocity Impact Test Final Report for Period," 1-15 April 2014, AEDC-TR-15-S-2, August 2015.
2. Shiotani, B., Rivero, M., Carrasquilla, M., Allen, S. "Characterizing DebriSat Fragments: So Many Fragments, So Much Data, and So Little Time," Proceeding 68th International Astronautical Congress, Adelaide, Australia, IAC-17.A6.3.6x41656, 2017.
3. Allen, S. "Characterizing DebriSat Fragments – Preliminary Results," Proceeding 69th International Astronautical Congress, Bremen, Germany, IAC-18.A6.3.4x45117, 2018.
4. Canny, J. "A Computational Approach to Edge Detection" IEEE Transactions on Pattern Analysis and Machine Intelligence, 8(6):679–698, 1986.
5. Rivero, M., Kleespies, J., Patankar, K., *et al*. "Characterization of Debris from the DebriSat Hypervelocity Tes,t" Proceedings 66th International Astronautical Congress, Jerusalem, Israel, IAC-15-A6.29x30343, 2015.
6. Adams, P.M., Sheaffer, P.M., Lingley, Z. and Radhakrishnan, G. "Characterization of Hypervelocity Impact Debris from the DebriSat Tests," Proceedings of the Advanced Maui Optical and Space Surveillance (AMOS) Technologies Conference, Wailea, Maui, Hawaii, September 19-22, 2017, Ed.: S. Ryan, The Maui Economic Development Board, Inc., id.56, 2017.
7. Dhawan, S. "A Review of Image Compression and Comparison of its Algorithms," International Journal of Electronics & Communication Technology, vol. 2, no. 1, pp. 22-26, March 2011.
8. Schäfer, S., Hiermaier, S., and Schneider, H. "Ballistic Limit Equation for the Normal Impact of Unyawed Ellipsoid-Shaped Projectiles on Aluminum Whipple Shields," 54th International Astronautical Congress, Bremen, American Institute of Aeronautics and Astronautics IAC-03-IAA.5.3.06, 2003.
9. Miller, J.E. "Considerations of Oblique Impacts of Non-Spherical, Graphite-Epoxy Projectiles," 1st International Orbital Debris Conference, Sugarland, TX, USA, 9-12 Dec. 2019.